LETTER Communicated by Michael Shadlen

Correlation Between Uncoupled Conductance-Based Integrate-and-Fire Neurons Due to Common and Synchronous Presynaptic Firing

Sybert Stroeve
Stan Gielen
Department of Biophysics, University of Nijmegen, 6525 EZ Nijmegen, The Netherlands

We investigate the firing characteristics of conductance-based integrate-and-fire neurons and the correlation of firing for uncoupled pairs of neurons as a result of common input and synchronous firing of multiple synaptic inputs. Analytical approximations are derived for the moments of the steady state potential and the effective time constant. We show that postsynaptic firing barely depends on the correlation between inhibitory inputs; only the inhibitory firing rate matters. In contrast, both the degree of synchrony and the firing rate of excitatory inputs are relevant. A coefficient of variation $CV > 1$ can be attained with low inhibitory firing rates and (Poisson-modulated) synchronized excitatory synaptic input, where both the number of presynaptic neurons in synchronous firing assemblies and the synchronous firing rate should be sufficiently large. The correlation in firing of a pair of uncoupled neurons due to common excitatory input is initially increased for increasing firing rates of independent inhibitory inputs but decreases for large inhibitory firing rates. Common inhibitory input to a pair of uncoupled neurons barely induces correlated firing, but amplifies the effect of common excitation. Synchronous firing assemblies in the common input further enhance the correlation and are essential to attain experimentally observed correlation values. Since uncorrelated common input (i.e., common input by neurons, which do not fire in synchrony) cannot induce sufficient postsynaptic correlation, we conclude that lateral couplings are essential to establish clusters of synchronously firing neurons.

1 Introduction

Correlated firing of cortical neurons has been observed in a series of experiments (Vaadia et al., 1995; Riehle, Grün, Diesman, & Aertsen, 1997; Singer & Gray, 1995), but opinions differ as to what extent such synchronization contributes to information representation and to information processing by ensembles of neurons (Philips & Singer, 1997) and about the contribution of the underlying mechanisms responsible for correlated firing. Broadly

speaking, correlated firing of neurons can be due to appropriate couplings between neurons in a network, due to common input to otherwise uncoupled neurons or, most likely, a combination of these two causes. The case of lateral couplings within a network has attracted a great deal of theoretical interest (van Vreeswijk, 1996; Ernst, Pawelzik, & Geisel, 1998; Bush & Sejnowski, 1996; Juergens & Eckhorn, 1997; Gerstner, 1998; Ermentrout & Kopell, 1998; Brunel & Hakim, 1999). These studies have shown that synchronization of the activity of neurons in a network arises in a large number of cases and that the correlation depends on the strength and dynamics of excitatory and inhibitory couplings.

Only a few studies have focused on the ontogenesis of correlated firing due to common input of uncoupled neurons. Feng, Brown, and Li (in press) proved that two noiseless leaky integrate-and-fire (IF) neurons with equal input streams in due time always synchronize perfectly; that is, the effect of the initial condition vanishes. This result was reported earlier by Knight (1972), but then synchronous firing was mostly considered an undesired artifact, which distorted the encoding of an input stimulus by the population firing rate. A drawback of the work by Feng et al. (in press) is that it considers 100% common input, which is not biologically plausible. A more general approach was taken by Shadlen and Newsome (1998), who simulated IF neurons with large numbers of excitatory and inhibitory synaptic input. These authors reported that the fractions of shared excitation and shared inhibition affect the correlation between firing of two neurons. They found only modest correlation, which led them to conclude that the temporal pattern of synaptic input could not be recovered from the pattern of output spikes. However, they considered only conditions of balanced excitatory and inhibitory input, which may not cover all possible biologically plausible cases of synaptic input. Diesmann, Gewaltig, and Aertsen (1999) showed that the propagation of synchronous spiking from one neural layer to the next due to excitatory common input can be described by attractor dynamics in the state-space of the number of spikes in a volley on the one hand and the temporal dispersion of the spikes on the other hand. The state-space portrait exhibits a basin of attraction such that large enough volleys with small enough dispersion survive in the propagation process.

In this article we study the effect of uncorrelated and correlated spiking of excitatory and inhibitory inputs on the firing characteristics of a single neuron and the effect of uncorrelated and correlated common input on the correlation of activity of a pair of neurons. In this analysis we use a conductance-based IF model, which is introduced in section 2. Simulations are required to obtain the firing behavior of the conductance-based IF neuron. Nevertheless, in section 3 we present relations for the mean and standard deviation of the steady-state membrane potential and the effective time constant that link the firing behavior with the model parameters. The effect of input correlation on the firing of a single neuron is analyzed in

section 4. Correlation between the firing of a pair of neurons with common input is studied in section 5. The results are discussed in section 6.

2 Model

2.1 Conductance-Based Integrate-and-Fire Model. The starting point for many neuron models is the leaky IF model, where a membrane current $I(t)$, being the sum of all incoming synaptic currents, charges a membrane capacitance C in parallel with a membrane resistance R:

$$\tau_m \dot{U}(t) = -U(t) + RI(t), \tag{2.1}$$

with $U(t)$ the membrane potential and $\tau_m = RC$ the membrane time constant. The neuron fires and resets its potential when the membrane potential exceeds the threshold U_t:

$$U(t^+) = U_r \text{ if } U(t) = U_t, \tag{2.2}$$

with $U_r < U_t$ the reset potential. A drawback of this model is that it assumes that the synapses act as independent current sources, implying that it neglects the decrease in the membrane resistance and the dependence of the effective time constant on the input spike rates (Koch, 1999). Since we want to study the correlation between the activity of neurons for a variety of input frequencies and input synchrony, the assumption of independent current sources is not justified in this context, and we will use a more plausible yet simple conductance-based IF model.

In this model, incoming spikes affect the conductance of channels for excitatory or inhibitory currents. The membrane equation is given by

$$C\dot{U}(t) = I_e(t) + I_i(t) + I_l(t), \tag{2.3}$$

where I_e, I_i, and I_l are the excitatory, inhibitory, and leak current, respectively:

$$I_e(t) = G_e(t)(E_e - U(t)) \tag{2.4}$$

$$I_i(t) = G_i(t)(E_i - U(t)) \tag{2.5}$$

$$I_l(t) = G_l(E_r - U(t)), \tag{2.6}$$

with E_e and E_i the excitatory and inhibitory reversal potentials, E_r the rest potential, and $G_e(t)$, $G_i(t)$, and G_l the excitatory, inhibitory, and leak conductance, respectively. These equations can be combined to:

$$\tau_m(t)\dot{U}(t) = -U(t) + U_\infty(t) \tag{2.7}$$

$$\tau_m(t) = \frac{C}{G_e(t) + G_i(t) + G_l} \tag{2.8}$$

$$U_\infty(t) = \frac{G_e(t)E_e + G_i(t)E_i + G_l E_r}{G_e(t) + G_i(t) + G_l}, \tag{2.9}$$

with U_∞ the steady-state potential and τ_m the effective time constant. The threshold-passing-plus-reset mechanism follows equation 2.2.

Neglecting spatial effects, the excitatory and inhibitory conductances depend on the recent input spiking times and are modeled by

$$G_e(t) = \sum_{j\in\Gamma_e}\sum_{f\in\mathcal{F}_j} g_e(t - t_j^f) \tag{2.10}$$

$$G_i(t) = \sum_{j\in\Gamma_i}\sum_{f\in\mathcal{F}_j} g_i(t - t_j^f), \tag{2.11}$$

with t_j^f the time of the fth spike of neuron j, Γ_e and Γ_i the set of excitatory and inhibitory synaptic inputs, respectively, $\mathcal{F}_j$ the set of firing instances, and g_e and g_i synaptic conductance functions. In this study, the synaptic conductance functions are pulses with a finite amplitude $\hat{g}$ and width τ:

$$g_{e,i}(t) = \begin{cases} 0 & t < 0 \\ \hat{g}_{e,i} & 0 \le t < \tau_{e,i} \\ 0 & t \ge \tau_{e,i}. \end{cases} \tag{2.12}$$

For an arbitrary constant membrane potential U_0 (compensating for the leak current), the change in membrane potential ΔU due to a conductance pulse approximately is

$$\Delta U \approx \tau\hat{g}(E - U_0)/C, \tag{2.13}$$

with E the appropriate (excitatory or inhibitory) reversal potential.

The following parameters are used in this article: $E_r = -75$ mV, $1/G_l = 40$ MΩ, $C = \tau_m G_l = 325$ pF with $\tau_m = 13$ ms, $U_t = E_r + 20 = -55$ mV, $E_i = -75$ mV, $E_e = 0$ mV, $\hat{g}_e = 1.2$ nS, $\tau_e = 1.5$ ms, $\hat{g}_i = 3.3$ nS, and $\tau_i = 1.5$ ms. The rest potential, threshold potential, input resistance, and time constant are in line with in vitro measurements on pyramidal neurons of the rat visual cortex by Mason, Nicoll, and Stratford (1991). The choice of the reversal potential of the excitatory and inhibitory synapses corresponds well to the work of Protopapas, Vanier, and Bower (1998). Notice that $E_i = E_r$, meaning that an inhibitory input at rest potential does not induce an inhibitory current. For the parameters chosen, it follows from equation 2.13 that an excitatory postsynaptic potential (EPSP) has a peak of 0.4 mV at the rest potential and 0.3 mV near the threshold potential. The peak potential, rise time, and half-width time are in line with the data of Mason et al. (1991). Near the threshold potential, an inhibitory postsynaptic potential (IPSP) has amplitude and rise time equal to an EPSP, that is, a peak of -0.3 mV (see equation 2.13) and a rise time of 1.5 ms. These results are in line with data of Matsumura, Chen, Sawaguchi, Kubota, and Fetz (1996), who reported about equal amplitudes and rise times for EPSPs and IPSPs. The simulations in this article use Euler integration with a time step $\Delta t = 0.1$ ms.

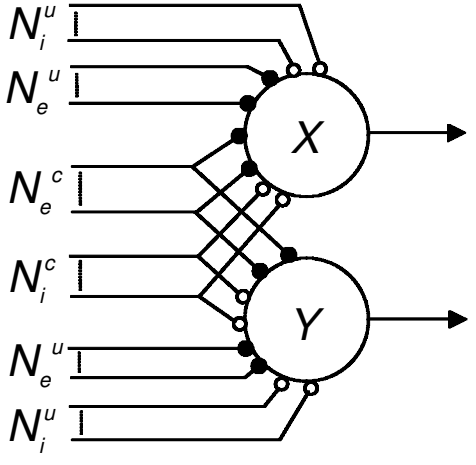

Figure 1: Neurons X and Y with unique and common excitatory (filled circles) and inhibitory (open circles) synapses. N_e^u and N_i^u are the number of unique excitatory and inhibitory inputs for each of the neurons X and Y. N_e^c and N_i^c are the number of common excitatory and inhibitory inputs, respectively.

2.2 Input Spike Series. We study the effects of synchronous presynaptic firing and partially common input on the induced firing statistics of a pair of neurons X and Y. The input signals of X and Y consist of six groups of spike series (see Figure 1): N_e^u and N_i^u unique excitatory and inhibitory inputs, respectively, for each of the neurons X and Y; N_e^c and N_i^c common excitatory and inhibitory inputs, respectively, for both X and Y. Fractions of excitatory (e) and inhibitory (i) common inputs are denoted by $\zeta_{e,i}$:

$$\zeta_{e,i} \equiv \frac{N_{e,i}^c}{N_{e,i}^u + N_{e,i}^c}. \tag{2.14}$$

In the absence of correlation between the input spike series, each spike series $s(t)$ can be considered as the result of an independent Poisson process. In the simulations, we apply the usual first-order approximation for the probability P_1 of a single spike in a small interval Δt of a process with firing frequency λ: $P_1 = \lambda \Delta t e^{-\lambda \Delta t} \approx \lambda \Delta t$. The assumption of a Poisson process ignores the effect of an (absolute) refractory period τ_r for the neurons, which provide input to neurons X and Y. For a single Poisson process, this simplification is justified if $\lambda \ll 1/\tau_r$, such that the probability of a spike in the refractory period is small: $P_1 \approx \lambda \tau_r \ll 1$. If the input consists of N Poisson processes with firing rate λ, then the effective input is a Poisson process with firing rate λN. If the total Poisson process generates two action potentials within the refractory period τ_r, then chances are approximately

$\lambda\tau_r/N$ that this happens due to the double firing of a single process and $(N-1)\lambda\tau_r/N$ that the event is caused by the firing of two processes. Following this first-order reasoning, this implies that the refractory period can be neglected if $\lambda \ll N/\tau_r$. For any reasonable choice of τ_r, N, and λ, this condition is fulfilled; for example, $\tau_r = 2\,\text{ms}, N = 100$ implies $\lambda \ll 5\ 10^4$ Hz.

The correlation between two spike series $s_x(t)$ and $s_y(t)$ is defined by

$$K_{xy}(\tau) \equiv \frac{\langle (s_x(t) - \langle s_x \rangle)(s_y(t+\tau) - \langle s_y \rangle) \rangle}{\sqrt{\langle (s_x(t) - \langle s_x \rangle)^2 \rangle \langle (s_y(t) - \langle s_y \rangle)^2 \rangle}}, \tag{2.15}$$

where $\langle s \rangle$ is the ensemble average of the spike process s, which is equal to the time average given the ergodicity of the process. In our study, correlation between synaptic inputs is taken into account by subdividing each set of excitatory or inhibitory synaptic inputs into synchronization clusters. In the visual system, neurons tend to fire in synchrony (Singer & Gray, 1995). Although there is some controversy about the functional significance of synchrony of firing, some authors have speculated that synchrony might serve as a label for neurons encoding the same object (this is called the binding hypothesis). Therefore, the idea was to investigate how various clusters of neurons, firing in synchrony while encoding the same object, might affect the firing of subsequent neurons. Therefore, a synchronization cluster was defined as follows. In the jth synchronization cluster, M_j presynaptic neurons fire independently according to Poisson processes with (background) rates $\lambda_j^b \equiv (1 - K_j)\lambda_j$ and fire synchronously according to a Poisson process with rate $\lambda_j^s \equiv K_j\lambda_j$. The total spike series is the "logical or" of the independent and the synchronous contributions. For $\lambda_j \Delta t \ll 1$ the resulting spike series have firing frequency λ_j and cluster correlation K_j; that is, the cross-correlation between two spike streams $s_q(t)$ and $s_r(t)$ $(q \neq r)$ in a synchronization cluster is given by

$$K_{qr}(\tau) = K_j \delta_1(\tau), \tag{2.16}$$

with $\delta_1(\tau) = 1$ for $\tau = 0$ and $\delta_1(\tau) = 0$ for $\tau \neq 0$. Each neuron is part of only one synchronization cluster, and there is no correlation between neurons in different synchronization clusters. In this study, we always use a firing rate λ_e equal for all excitatory inputs and a firing rate λ_i equal for all inhibitory inputs. Furthermore, we apply equal numbers of excitatory and inhibitory inputs $N_e = N_i = 120$. For simplicity, the inputs are divided in clusters of equal size M, and the cluster correlation is K_e for excitatory inputs and K_i for inhibitory inputs.

In conclusion, the relevant variables of the input spike series are the excitatory and inhibitory firing rates λ_e and λ_i, the fractions of excitatory and inhibitory common inputs ζ_e and ζ_i, the cluster size M, and the excitatory and inhibitory cluster delta correlations K_e and K_i.

3 Single Neuron with Independent Inputs

3.1 Analytical Results. A analytical expression for the firing characteristics is known only for the nonleaky IF model (see equation 2.1 with $R = \infty$) (Tuckwell, 1988). For leaky IF models, numerical calculations are necessary to obtain a solution for the threshold-passing problem. Some insight into the firing characteristics of a leaky IF model can be obtained by calculating the mean and variance of the membrane potential while neglecting the threshold-passing-reset mechanism. Results of such calculations for the current-based IF model of equation 2.1 are presented in Tuckwell (1988) and Koch (1999). In this article, we derive expressions for the moments of the steady-state potential and time constant of the conductance-based IF model.

The total excitatory and inhibitory conductances G_e and G_i are the sums of the synaptic conductance pulses over all synapses and (recent) spike times (see equations 2.10 and 2.11). Since the input spike trains are Poisson processes, the sums are Poisson distributions too. For the case of independent inputs, the resulting distributions have frequencies $\nu_e \equiv N_e\lambda_e\tau_e$ and $\nu_i \equiv N_i\lambda_i\tau_i$, leading to mean conductances $\langle G_e\rangle = \hat{g}_e\nu_e$ and $\langle G_i\rangle = \hat{g}_i\nu_i$ for the excitatory and inhibitory processes, respectively. If $\nu_{e,i} \gg 1$, these Poisson distributed total conductances are well described by gaussian processes with means $\mu_e \equiv \hat{g}_e\nu_e$ and $\mu_i \equiv \hat{g}_i\nu_i$ and standard deviations $\sigma_e \equiv \hat{g}_e\sqrt{\nu_e}$ and $\sigma_i \equiv \hat{g}_i\sqrt{\nu_i}$. For simplicity, we use $N_e = N_i = 120$ and vary the excitatory and inhibitory firing rates to achieve various ratios of excitation to inhibition.

The moments of the steady-state potential U_∞ and the time constant τ_m can be calculated exactly using the definition of the expectation of a function of two independent Poisson processes:

$$\langle\gamma\rangle = \sum_{k=0}^{\infty}\sum_{l=0}^{\infty}\gamma\,(\hat{g}_e k, \hat{g}_i l)\, e^{-\nu_e}\frac{\nu_e^k}{k!}\, e^{-\nu_i}\frac{\nu_i^l}{l!}, \tag{3.1}$$

with γ the appropriate function (e.g., see equations 2.8 or 2.9). Figure 2 shows the analytically exact results for the mean and standard deviation of the steady-state potential U_∞ and the effective membrane time constant τ_m.

Approximate relations for the mean and standard deviation of the steady-state potential and time constant can be derived by using the gaussian approximation for the sum of a large number of Poisson processes and analytically integrating a first-order approximation of the function γ :

$$\langle\gamma\rangle = \frac{1}{2\pi\,\sigma_e\sigma_i}\int_{-\infty}^{\infty}\int_{-\infty}^{\infty}\gamma\,(x,y)\exp\left(-\frac{(x-\mu_e)^2}{2\sigma_e^2}\right)\exp\left(-\frac{(y-\mu_i)^2}{2\sigma_i^2}\right) \times dx\,dy \tag{3.2}$$

$$= \frac{1}{2\pi\,\sigma_e\sigma_i}\int_{-\infty}^{\infty}\int_{-\infty}^{\infty}\exp\left\{\log\gamma\,(x,y) - \frac{(x-\mu_e)^2}{2\sigma_e^2} - \frac{(y-\mu_i)^2}{2\sigma_i^2}\right\} \times dx\,dy \tag{3.3}$$

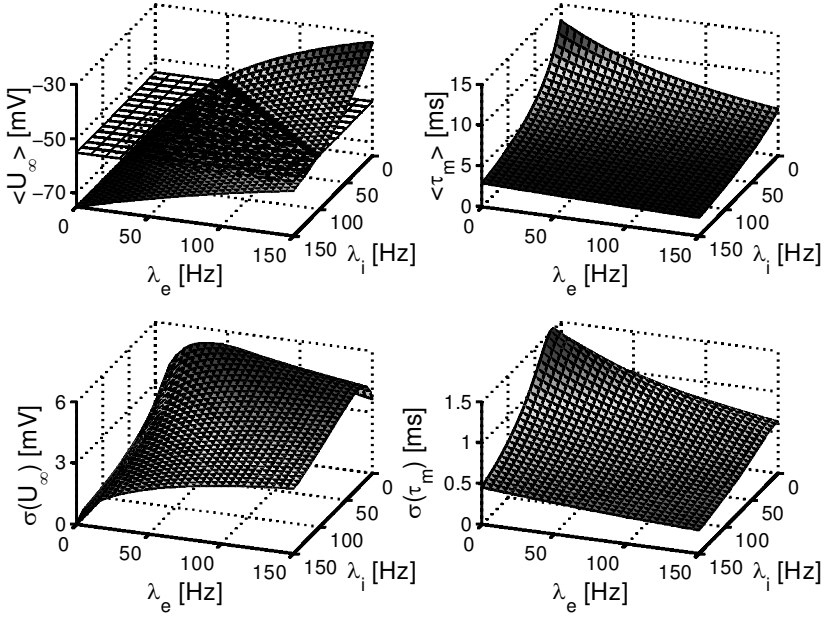

Figure 2: Results of exact analytical calculations (see equation 3.1) of the mean (top) and standard deviation (bottom) of the steady-state potential U_∞ (left) and time-constant τ_m (right) as a function of the excitatory (λ_e) and inhibitory (λ_i) firing rate for the conductance-based IF model. These exact results were calculated using equation 3.1. The horizontal flat grid in the upper left graph represents the threshold potential $U_t = -55$ mV. Its intersection with the curved surface of $\langle U_\infty \rangle$ is emphasized by a thick line. In the other graphs, the solid line represents the values of $\langle \tau_m \rangle$, $\sigma(U_\infty)$, $\sigma(\tau_m)$ for the values of λ_e and λ_i, corresponding to $\langle U_\infty \rangle = U_t$.

$$\approx \frac{1}{2\pi\sigma_e\sigma_i}\int_{-\infty}^{\infty}\int_{-\infty}^{\infty}\exp\left\{\log\gamma\,(\mu_e,\mu_i) + (x-\mu_e)\frac{1}{\gamma}\frac{\partial\gamma}{\partial x}\bigg|_{\mu_e,\mu_i} + (y-\mu_i)\frac{1}{\gamma}\frac{\partial\gamma}{\partial y}\bigg|_{\mu_e,\mu_i} - \frac{(x-\mu_e)^2}{2\sigma_e^2} - \frac{(y-\mu_i)^2}{2\sigma_i^2}\right\}dx\,dy \tag{3.4}$$

$$= \gamma\,(\mu_e,\mu_i)\exp\left\{\frac{1}{2\gamma\,(\mu_e,\mu_i)^2}\left(\sigma_e^2\left(\frac{\partial\gamma}{\partial x}(\mu_e,\mu_i\right)\right)^2 + \sigma_i^2\left(\frac{\partial\gamma}{\partial y}(\mu_e,\mu_i)\right)^2\right)\right\} \tag{3.5}$$

The following equations were derived with this method:

$$\langle U_\infty \rangle \approx \frac{E_e\mu_e + E_i\mu_i + E_rG_l}{\mu_e + \mu_i + G_l} \exp\left(\frac{\sigma_e^2\xi_e^2 + \sigma_i^2\xi_i^2}{2}\right) \tag{3.6}$$

$$\sigma(U_\infty) \approx \left|\frac{E_e\mu_e + E_i\mu_i + E_rG_l}{\mu_e + \mu_i + G_l}\right| \times \sqrt{\exp(2(\sigma_e^2\xi_e^2 + \sigma_i^2\xi_i^2)) - \exp(\sigma_e^2\xi_e^2 + \sigma_i^2\xi_i^2)} \tag{3.7}$$

$$\xi_e = (E_e(\mu_i + G_l) - E_i\mu_i - G_lE_r) \times \left(E_e\mu_e^2 + G_l(E_e + E_r)\mu_e + (E_e + E_i)\mu_e\mu_i + G_l(E_i + E_r)\mu_i + E_i\mu_i^2 + E_rG_l^2\right)^{-1} \tag{3.8}$$

$$\xi_i = (E_i(\mu_e + G_l) - E_e\mu_e - G_lE_r) \times \left(E_e\mu_e^2 + G_l(E_e + E_r)\mu_e + (E_e + E_i)\mu_e\mu_i + G_l(E_i + E_r)\mu_i + E_i\mu_i^2 + E_rG_l^2\right)^{-1} \tag{3.9}$$

$$\langle \tau_m \rangle \approx \frac{C}{\mu_e + \mu_i + G_l} \exp\left(\frac{\sigma_e^2 + \sigma_i^2}{2(\mu_e + \mu_i + G_l)^2}\right) \tag{3.10}$$

$$\sigma(\tau_m) \approx \frac{C}{\mu_e + \mu_i + G_l} \times \sqrt{\exp\left(\frac{2(\sigma_e^2 + \sigma_i^2)}{(\mu_e + \mu_i + G_l)^2}\right) - \exp\left(\frac{\sigma_e^2 + \sigma_i^2}{(\mu_e + \mu_i + G_l)^2}\right)}. \tag{3.11}$$

The mean and maximum absolute differences between the exact statistics shown in Figure 2 and the values obtained by equations 3.6 through 3.11 are 0.18 and 0.34 mV for $\langle U_\infty \rangle$, 0.04 and 0.13 mV for $\sigma(U_\infty)$, 0.05 and 0.12 ms for $\langle \tau_m \rangle$, and 0.02 and 0.10 ms for $\sigma(\tau_m)$, respectively. The zeroth-order approximations of the mean values (excluding the exponential function in equations 3.6 and 3.10) are fairly accurate with mean and maximum errors of 0.11 and 0.53 mV, and 0.05 and 0.12 ms, respectively. This illustrates that equations 3.6 through 3.11 provide a good approximation to the exact results.

What do these statistical moments tell us about the firing characteristics of the neuron? Clearly, if the steady-state potential $U_\infty(t)$ is below the threshold level U_t, then $U(t) < U_t$, and no firing can occur. Comparison of $\langle U_\infty \rangle$ with U_t in connection with its standard deviation $\sigma(U_\infty)$ therefore provides insight into the neuron's firing characteristics. We first consider the case for which $\langle U_\infty \rangle = U_t$. The solid line in the upper left panel of Figure 2 represents the relation between λ_e and λ_i for this case. Using the zeroth-order approximation of $\langle U_\infty \rangle$, an analytical relation for this line can easily be derived:

$$\lambda_i = \phi(\lambda_e) = \frac{\lambda_e N_e \hat{g}_e \tau_e (E_e - U_t) - G_l(U_t - E_r)}{N_i \hat{g}_i \tau_i (U_t - E_i)} \equiv a_\phi \lambda_e - b_\phi. \tag{3.12}$$

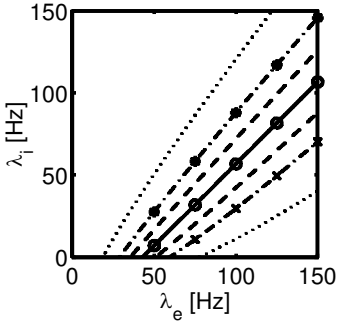

Figure 3: The inhibitory frequency λ_i for which $\langle U_\infty \rangle = U_t + k\sigma(U_\infty)$ as a function of the excitatory frequency λ_e. Solid line with circles: $k = 0$; dashed lines: $k = \pm 0.5$; dash-dotted line with crosses: $k = 1$; dash-dotted line with asterisks: $k = -1$; dotted lines: $k = \pm 2$. Inhibitory firing rates λ_i with $k > 0$ imply frequent and regular firing; firing rates λ_i with $k < 0$ imply rare and irregular firing (see also Figure 4).

Notice that $\phi(\lambda_e)$ can be negative due to the offset b_ϕ, implying that $\langle U_\infty \rangle < U_t$, even in the absence of inhibition. Now, if $\lambda_i \ll \phi(\lambda_e)$, then $\langle U_\infty \rangle \gg U_t$. Therefore, being almost independent from variations in U_∞, output firing is regular. In this case, the mean interspike interval (ISI) can be approximated by the deterministic case, where the ISI is set by the threshold potential U_t, the reset potential U_r, the time constant τ_m, and the steady-state potential U_∞, following the solution of the first-order differential equation:

$$U_t - U_r = (1 - \exp(-\mathrm{ISI}/\tau_m))(U_\infty - U_r). \tag{3.13}$$

Setting $\tau_m = \langle \tau_m \rangle$, $U_\infty = \langle U_\infty \rangle$, and $\mathrm{ISI} = \langle \mathrm{ISI} \rangle$ we obtain the (upper bound) approximation:

$$\langle \mathrm{ISI} \rangle \approx \langle \tau_m \rangle \log\left(\frac{\langle U_\infty \rangle - U_r}{\langle U_\infty \rangle - U_t}\right). \tag{3.14}$$

On the other hand, if $\lambda_i \gg \phi(\lambda_e)$, then $\langle U_\infty \rangle \ll U_t$, and output firing is rare and irregular.

A more general picture evolves if we also include the variation of U_∞ in this analysis, which also depends on λ_i and λ_e. Figure 3 shows the inhibitory frequencies λ_i for which $\langle U_\infty \rangle = U_t + k\sigma(U_\infty)$ with $k \in \{0, \pm 0.5, \pm 1, \pm 2\}$ as a function of λ_e. We denote these inhibitory frequencies as $\lambda_i^t(k, \lambda_e)$, or sometimes simply as $\lambda_i^t(k)$. It follows from Figure 3 that the lines representing $\lambda_i^t(k, \lambda_e)$ for different values of k diverge. This implies that the intermediate frequency regime, where $\lambda_i^t(k, \lambda_e) \leq \lambda_i \leq \lambda_i^t(-k, \lambda_e)$, becomes larger for increasing excitatory firing rates.

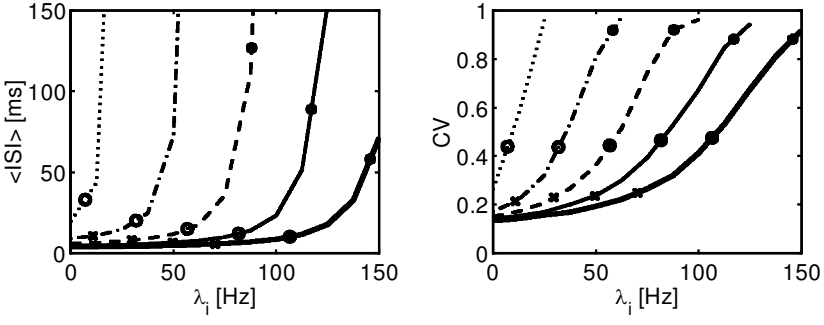

Figure 4: Results of numerical simulations, showing mean ISI and CV as a function of inhibitory firing frequency λ_i for a series of excitatory frequencies: $\lambda_e = 50$ Hz (dotted line), $\lambda_e = 75$ Hz (dash-dotted line), $\lambda_e = 100$ Hz (dashed line), $\lambda_e = 125$ Hz (solid line), $\lambda_e = 150$ Hz (thick solid line). Circles denote the points where $\langle U_\infty \rangle = U_t$, crosses denote the points where $\langle U_\infty \rangle = U_t + \sigma(U_\infty)$, and asterisks denote the points where $\langle U_\infty \rangle = U_t - \sigma(U_\infty)$ (see also Figure 3). Averages are based on 10,000 spikes.

3.2 Numerical Simulations. Now we proceed from the analytical results to simulation results of the conductance-based IF model and thereby link the function $\lambda_i^t(k, \lambda_e)$ to the spiking behavior of the neuron. Figure 4 shows the mean interspike interval $\langle \mathrm{ISI} \rangle$ and its coefficient of variation CV as a function of the excitatory and inhibitory firing rates. For increasing inhibitory frequency, $\langle \mathrm{ISI} \rangle \to \infty$ and $\mathrm{CV} \to 1$. For low inhibitory firing rates, $\langle \mathrm{ISI} \rangle$ is small and CV is relatively small, indicating that firing of the output neuron is frequent and regular. The incline of the graphs becomes less steep for higher excitatory firing rates. This is related to the increase in the intermediate frequency regime $\lambda_i^t(k, \lambda_e) \le \lambda_i \le \lambda_i^t(-k, \lambda_e)$ for large λ_e, shown in Figure 3. The stars, circles, and crosses denote the approximate mean ISI and CV for which $\langle U_\infty \rangle = U_t + k\sigma(U_\infty)$ with $k \in \{-1, 0, 1\}$, respectively. The CV for a particular value of k is approximately constant with $\mathrm{CV}(k = 1) \approx 0.23$, $\mathrm{CV}(k = 0) \approx 0.45$, and $\mathrm{CV}(k = -1) \approx 0.90$. However, the mean ISI for constant k decreases for larger λ_e. This can, at least partly, be explained by the fact that the mean effective time constant $\langle \tau_m \rangle$ decreases for increasing excitatory and inhibitory firing rates (see Figure 2). A small time constant implies a short rise time of the membrane potential toward the threshold potential.

Figure 5 shows the prespike averages of the total synaptic conductances, the membrane potential, the steady-state potential, and the time constant for an excitatory firing rate $\lambda_e = 100$ Hz and for two inhibitory firing rates: $\lambda_i = \lambda_i^t(1) = 29.6$ Hz (implying $\langle U_\infty \rangle = U_t + \sigma(U_\infty)$) and $\lambda_i = \lambda_i^t(-1) = 88.0$ Hz (implying $\langle U_\infty \rangle = U_t - \sigma(U_\infty)$). In addition to the mean value plus

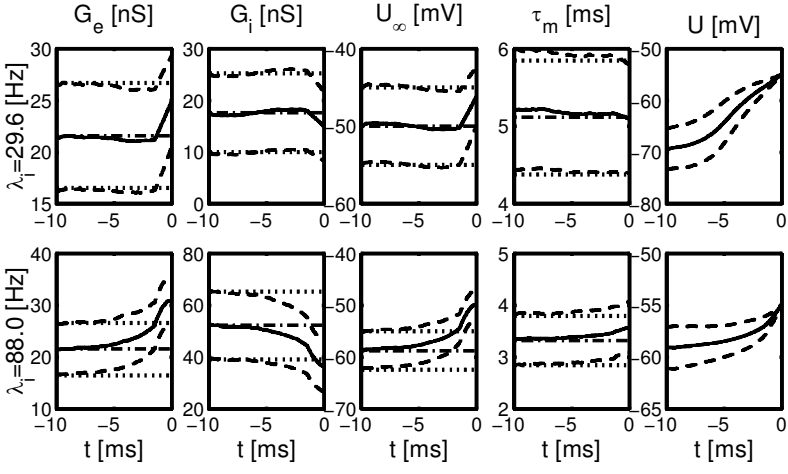

Figure 5: Mean and standard deviation of prespike conductances G_e and G_i, steady-state potential U_∞, time constant τ_m, and membrane potential U for uncorrelated inputs ($N_e = N_i = 120$, $\lambda_e = 100$ Hz) and two inhibitory firing rates: $\lambda_i = \lambda_i^t(1, \lambda_e) = 29.6$ Hz (top row) and $\lambda_i = \lambda_i^t(-1, \lambda_e) = 88.0$ Hz (bottom row). The solid and dashed lines represent the prespike mean ± SD, averaged over 10,000 spikes in numerical simulations. The dash-dotted and dotted lines represent the mean ± SD of approximated conductances, steady-state potential, and time constant calculated by equations 3.6 through 3.11. The threshold potential is $U_t = -55$ mV.

or minus the standard deviation of the simulation results (solid and dashed lines), the graphs show the mean plus or minus the standard deviation (dash-dotted and dotted lines) of the approximated statistics according to equations 3.6 through 3.11. For large enough prespike times ($t \leq -5$ ms) the simulated and approximated values correspond well. For $\lambda_i = 29.6$ Hz, the above-threshold value of $\langle U_\infty \rangle$ leads to a constant increase in the membrane potential U and to regular and fast firing: $\langle \text{ISI} \rangle = 8.0$ ms, CV $= 0.23$ (see the crosses on the dashed lines in Figure 4). This mean ISI compares well with $\langle \text{ISI} \rangle = 8.2$ ms obtained with equation 3.14. Spiking is on average preceded by a small increase in U_∞. For $\lambda_i = 88.0$ Hz, the steady-state potential $\langle U_\infty \rangle$ is below threshold, output spiking is rare and irregular ($\langle \text{ISI} \rangle = 116$ ms, CV $=$ 0.89, as is indicated by the asterisks on the dashed lines in Figure 4), and the temporary conductance changes are necessary to induce spiking. Just before spiking, the excitatory conductance exceeds its nonspiking mean value (i.e., the mean value for $t \approx -10$ ms) by about twice its standard deviation, and the inhibitory conductance undershoots its nonspiking mean value by more than the standard deviation. For both inhibitory firing rates, the time constant τ_m before an action potential reveals only small variations. This can

be explained by the fact that, on average, firing is associated with both an excitatory conductance increase and an inhibitory conductance decrease.

4 Single Neuron with Correlated Inputs

For our analysis of the effects of input correlation on the firing characteristics of a single neuron, we choose a single excitatory firing rate $\lambda_e = 100$ Hz and vary:

1. The inhibitory firing rate $\lambda_i \in \{0.0, 29.6, 56.7, 88.0\}$, representing the cases no inhibition, $\langle U_\infty \rangle = U_t + \sigma(U_\infty)$, $\langle U_\infty \rangle = U_t$, and $\langle U_\infty \rangle = U_t - \sigma(U_\infty)$, respectively.
2. The cluster correlation $K_{e,i} \in \{0.05, 0.10, 0.20, 0.40\}$, indicating that the firing rate of neurons in a synchronization cluster is $\lambda^s_{e,i} = \lambda_{e,i} K_{e,i}$ and that the background firing rate is $\lambda^b_{e,i} = \lambda_{e,i}(1 - K_{e,i})$.
3. The cluster size $M \in \{15, 30, 60, 120\}$, indicating that the size of a synchronization cluster can be 12.5%, 25%, 50%, or 100% of the total number of excitatory or inhibitory inputs.

The firing statistics were simulated for these 64 cases (4 inhibitory firing rates $\times$ 4 cluster correlations $\times$ 4 cluster sizes) with correlation in both excitatory and inhibitory clusters (see Figure 6), correlation only in excitatory clusters (see Figure 7), and correlation only in inhibitory clusters (see Figure 8).

A number of characteristic features can be observed in Figures 6, 7, and 8. The upper panels show that in all cases, $\langle \text{ISI} \rangle$ is remarkably insensitive for changes in both the cluster correlation K and the cluster size M, except for the high inhibitory firing rate $\lambda_i = \lambda^t_i(-1) = 88$ Hz, when $\langle \text{ISI} \rangle$ decreases for larger values for the cluster correlation K. The decrease in Figures 6 and 7 for $\lambda_i = 88$ Hz can be explained by the fact that long-lasting fluctuations of the membrane potential near $\langle U_\infty \rangle$ (remember $\langle U_\infty \rangle < U_t$) are prevented by the synchronous firing of the excitatory clusters, and more frequent firing of those clusters thus reduces $\langle \text{ISI} \rangle$. If $\langle U_\infty \rangle \geq U_t$ (for $\lambda_i \in \{0.0, 29.6, 56.7\}$ Hz), presynaptic excitatory cluster firing is also likely to induce threshold passing, but since regular firing is already caused by the background firing and since the total excitatory firing rate $\lambda_e = \lambda^s_e + \lambda^b_e$ is constant, the mean ISI is hardly reduced in this case. The decrease in $\langle \text{ISI} \rangle$ as a function of the inhibitory correlation in Figure 8 can be understood by noting that an increase in the cluster correlation is associated with a decrease in the inhibitory background activity. Thus, inhibitory activity is most effective in reducing the firing rate of the postsynaptic neuron, if it is independent.

In contrast to the firing rate, CV clearly depends on the input correlation for all inhibitory firing rates, except if only the inhibitory inputs are correlated (in Figure 8). Figures 6 and 7 show a very similar dependency of CV on the input correlation: larger cluster sizes and larger cluster correlation tend to increase CV, except for high inhibitory firing rates, where a rise in

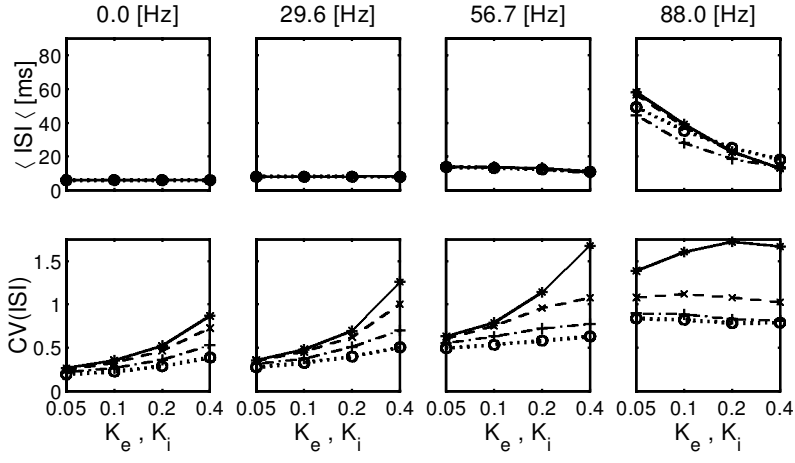

Figure 6: Firing characteristics of a single neuron with excitatory correlation and inhibitory correlation. ⟨ISI⟩ and CV as a function of cluster correlation K_e and K_i, for excitatory firing $\lambda_e = 100$ Hz and a series of inhibitory firing frequencies $\lambda_i \in \{0, 29.6, 56.7, 88.0\}$ Hz (columns 1–4). The cluster size M varies from 12.5% to 100% of the number of excitatory and inhibitory inputs ($N_e = N_i = 120$): $M = 15$ (dotted line, circles), $M = 30$ (dash-dotted line, pluses), $M = 60$ (dashed line, crosses), $M = 120$ (solid line, asterisks). Both excitatory and inhibitory clusters are correlated, but excitatory and inhibitory inputs are independent. Averages are over 10,000 spikes.

the cluster correlation does not always lead to an increase in CV. In these simulations, large cluster sizes are required to achieve CV > 1, but the inhibitory firing rates may be relatively low. If only the inhibitory inputs are correlated (see Figure 8), CV is mostly independent of the input correlation, except for $\lambda_i = \lambda_i^t(-1)$, where a slight decrease in CV as a function of cluster size and correlation can be observed. This decrease is associated with the decrease in the effect of the independent inhibitory input.

5 Uncoupled Neurons with Common Input

We now consider the correlation between the firing of two neurons with partially common excitatory and/or inhibitory input sources without correlation in the input streams of each single neuron (cluster correlation $K = 0$). Figure 9 shows the cross-correlation of neural activity of two neurons with both common excitatory and inhibitory sources for various ratios of common input, and both for a low ($\lambda_i = 30$ Hz) and a high ($\lambda_i = 90$ Hz) inhibitory frequency. These frequencies are close to the firing rates for which $\langle U_\infty \rangle = U_t \pm \sigma(U_\infty)$. The cross-correlation functions reveal three character-

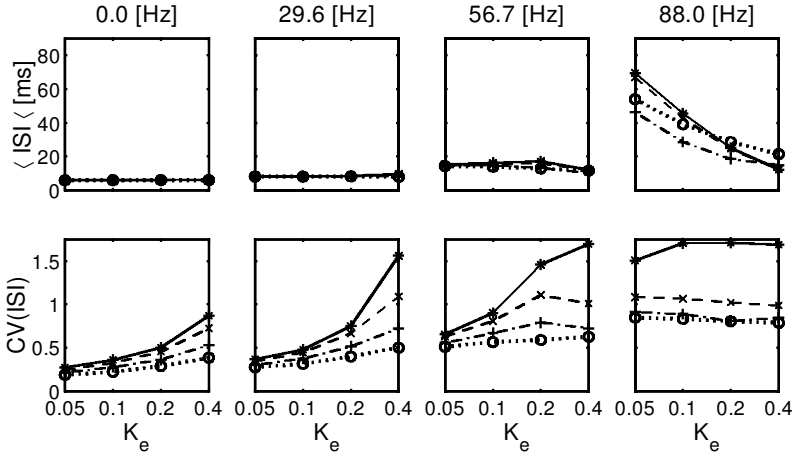

Figure 7: Firing characteristics of a single neuron with excitatory correlation. ⟨ISI⟩ and CV as a function of cluster correlation K_e, for excitatory firing $\lambda_e = 100$ Hz and a series of inhibitory firing frequencies $\lambda_i \in \{0, 29.6, 56.7, 88.0\}$ Hz (columns 1–4). The cluster size M varies from 12.5% to 100% of the number of excitatory inputs ($N_e = N_i = 120$): $M = 15$ (dotted line, circles), $M = 30$ (dash-dotted line, pluses), $M = 60$ (dashed line, crosses), $M = 120$ (solid line, asterisks). Only excitatory inputs are correlated. Averages are over 10,000 spikes.

istics. First, the cross-correlation is oscillatory for $\lambda_i = 30$ Hz, whereas it has only a single central peak for $\lambda_i = 90$ Hz. The oscillatory cross-correlation for $\lambda_i = 30$ Hz is due to the small coefficient of variation (CV ≈ 0.23; see Figure 4) of the neurons with low inhibitory input. This implies that after synchronous spiking of neurons X and Y due to the common input, there is a large probability that both neurons will fire again after a time ⟨ISI⟩. The oscillation frequency of $K_{xy}(\tau)$ thus equals $\langle \mathrm{ISI} \rangle^{-1}$. For $\lambda_i = 90$ Hz the CV is much higher (near one; see Figure 4), and therefore the cross-correlation is not oscillatory. Second, the zero-time cross-correlation $K_{xy}(0)$ increases with the proportion of common input (as expected). Third, for the same common contribution, $K_{xy}(0)$ is larger for increased inhibitory firing. The more general picture of this phenomenon becomes clear from the graphs in Figure 10. These show zero-time cross-correlation $K_{xy}(0)$ as a function of the inhibitory firing frequency and the amount of common input for pairs of neurons with only common excitatory input (A), only common inhibitory input (C), and both common excitatory and inhibitory inputs (B).

Figure 10A shows that $K_{xy}(0)$ increases for larger amounts of common excitatory contributions. It also increases for small inhibitory firing rates, reaching an optimum at about $\lambda_i \approx 75$ Hz. The maximum correlation,

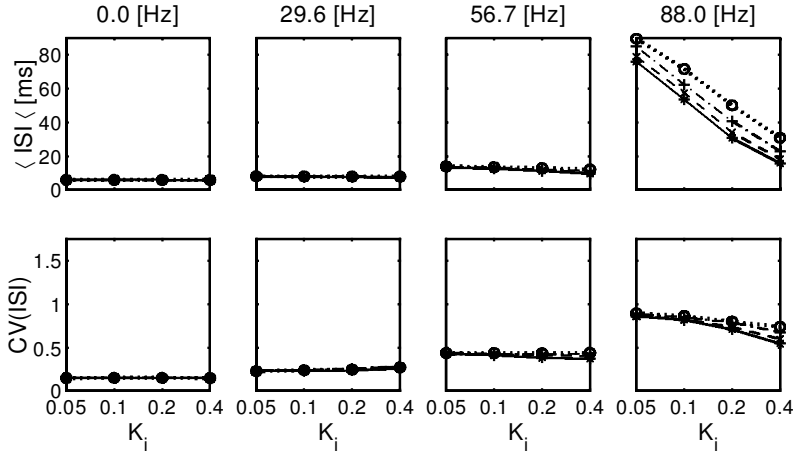

Figure 8: Firing characteristics of a single neuron with inhibitory correlation. $\langle \text{ISI} \rangle$ and CV as a function of cluster correlation K_i, for excitatory firing $\lambda_e = 100$ Hz and a series of inhibitory firing frequencies $\lambda_i \in \{0, 29.6, 56.7, 88.0\}$ Hz (columns 1–4). The cluster size M varies from 12.5% to 100% of the number of inhibitory inputs ($N_e = N_i = 120$): $M = 15$ (dotted line, circles), $M = 30$ (dash-dotted line, pluses), $M = 60$ (dashed line, crosses), $M = 120$ (solid line, asterisks). Only inhibitory inputs are correlated. Averages are over 10,000 spikes.

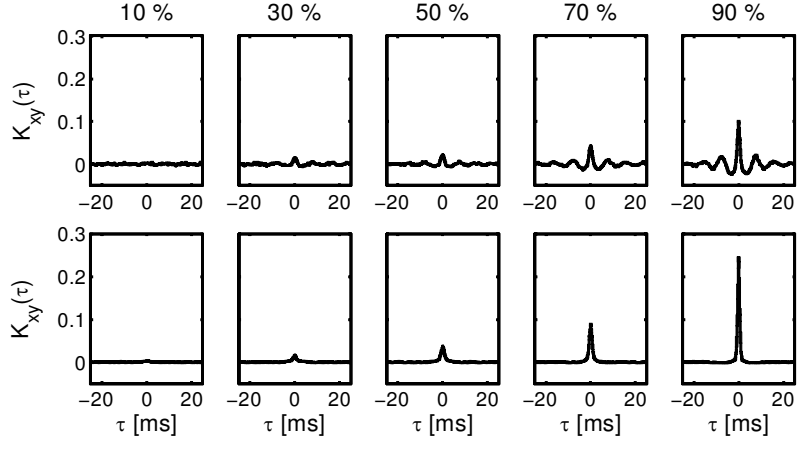

Figure 9: Cross-correlation $K_{xy}(\tau)$ between output spikes of two conductance-based IF neurons X and Y with partially common excitatory ($\lambda_e = 100$ Hz) and inhibitory input (upper row: $\lambda_i = 30$ Hz, bottom row: $\lambda_i = 90$ Hz). The columns represent 10%, 30%, 50%, 70%, and 90% common excitatory and inhibitory input. Averages are over 16,500 to 25,000 spikes; bin size is 0.5 ms.

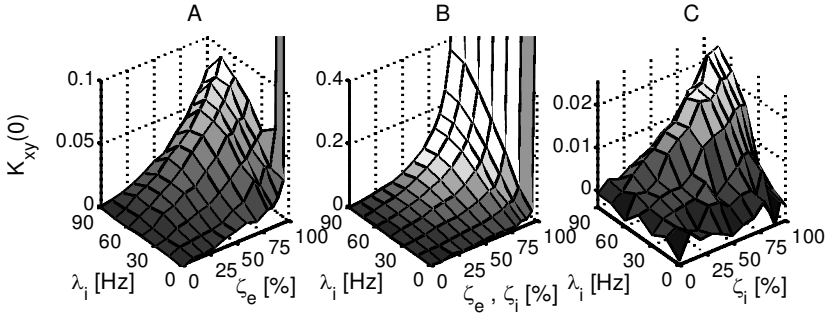

Figure 10: Cross-correlation $K_{xy}(0)$ at time zero between the output spikes of two conductance-based IF neurons with partially common excitatory ($\lambda_e = 100$) and inhibitory input as a function of the common contribution and the inhibitory firing rate λ_i. (A) Only common excitatory input. (B) Both common excitatory and inhibitory input. (C) Only common inhibitory input. Notice that the z-axes differ. Averages are over 16,500 to 25,000 spikes; bin size is 0.5 ms.

which is attained for 100% common excitatory input and near $\lambda_i = 75$ Hz, is $K_{xy}(0) = 0.092$. Notice that this value is much lower than the maximum value ($K_{xy}^{\max} = 1$) due to the completely independent inhibitory inputs. How can we understand the initial incline of $K_{xy}(0)$ with increasing λ_i and the decrease of $K_{xy}(0)$ for large λ_i? We observed in section 3 that an increase in the (independent) inhibitory input induces an increase in $\langle$ISI$\rangle$ and CV, reflecting that firing requires the coincidence of a momentary increase in excitatory input and/or a decrease in inhibitory input. The timing of excitatory input pulses is thus more important under the influence of inhibitory firing. The effect of coincidental excitatory synchronous firing of common inputs becomes more effective for larger inhibitory firing, leading to the initial increase in the cross-correlation. For large inhibitory firing rates, postsynaptic firing requires both an increase in the excitation and a decrease in the inhibition. Since the inhibitory firing series for the two neurons were chosen to be independent for the simulations shown in Figure 10A, this implies that the cross-correlation decreases for large inhibitory firing rates.

Figure 10B shows that common inhibition strongly amplifies the effect of common excitation, that is, $K_{xy}(0)$ is larger if both common excitatory and inhibitory signals are present. This can be understood by the notion that common inhibition tends to create an equal baseline level from which common excitation has an equal depolarizing effect on both neurons. Clearly, the increase is largest if $\zeta_e = \zeta_i$ tend to 100%, but a considerable increase of 77% is already attained for $\zeta_e = \zeta_i = 50\%$.

The results in Figure 10C show that common inhibition alone induces only a small correlation between the firing events, giving a peak cross-

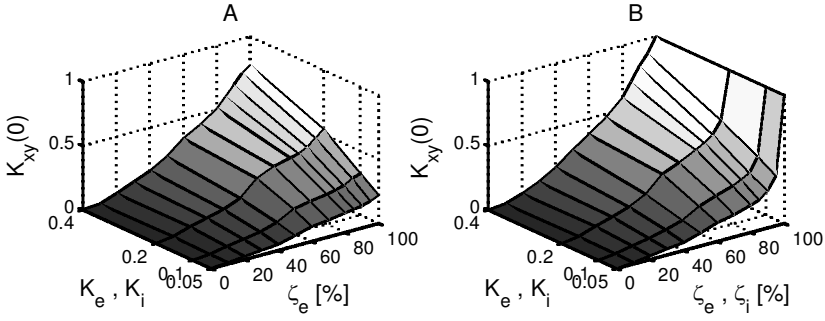

Figure 11: Cross-correlation $K_{xy}(0)$ at time zero between output spikes of two conductance-based IF neurons with excitatory and inhibitory input (λ_e = 100 Hz, λ_i = 60 Hz) and partially common input as a function of the common contributions $\zeta_{e,i}$ and the cluster correlations $K_{e,i}$. Each of the six input groups represents a cluster. (A) Only excitatory common input. The input correlation leads to a large increase in $K_{xy}(0)$ (compare with Figure 10A). (B) Both excitatory and inhibitory common input. Averages are over 25,000 spikes; bin size is 0.5 ms.

correlation $K_{xy}(0) = 0.026$. Although an equal baseline is set by the common inhibition, the independent excitatory input is most important to pass the threshold potential. Common inhibition is thus effective only in increasing the cross-correlation in the presence of common excitation.

How is the correlation between firing of a pair of neurons affected by synchronization clusters in the input streams? Figure 11 shows the correlation between the spiking of two uncoupled neurons with partially common input and correlation between the neurons in a cluster. The inhibitory firing rate λ_i is set to 60 Hz with $N_e = N_i = 120$ and $\lambda_e = 100$ Hz. The cluster sizes are maximum; all six groups of inputs (excitatory/inhibitory, 2× unique, 1× common) form a cluster. This implies that the cluster sizes vary as a function of the amount of common input. Comparison of the results in Figure 11 and Figures 10A and 10B (for $\lambda_i = 60$ Hz) leads to the conclusion that the cross-correlation is strongly enhanced by the input correlation, which now comprises both a spatial component (the common inputs) and a temporal component (the cluster synchronization). For instance, 20% common input leads to a correlation peak of 0.013 without synchronous inputs, whereas a correlation peak of 0.06, about five times larger, is attained for input correlation $K = 0.1$.

6 Discussion

6.1 Pros and Cons of the Neuron Model. The conductance-based IF model is an extension of the leaky current-based IF model, which uses con-

ductance pulses instead of current pulses to drive the membrane potential. It is more in line with experimental data and adds the feature of variation of the effective time constant, which may be important in the study of timing effects of the neuron's input. For both the conductance-based and the current-based leaky IF model, one has to rely on simulations to characterize its firing behavior. Nevertheless, relations for the first and second moments of the membrane potential for the current-based IF model (Tuckwell, 1988) and for the moments of the steady-state potential and the effective time constant of the conductance-based IF model (this article) provide an analytical link between pre- and postsynaptic firing. Only for the nonleaky IF model are analytical expressions of its firing behavior known (Tuckwell, 1988). However, having infinite memory, the nonleaky IF model is not useful for a study on the effects of synchronous input (Kempter, Gerstner, van Hemmen, & Wagner, 1998) or for a study on correlation due to common input, since even in the case of 100% common input, synchronous firing is achieved only if the initial conditions are identical in the absence of noise.

The statistical moments of the steady-state potential and the time constant were derived by assuming that a spike induces a constant and finite increase in the conductance for a short time. Such a conductance pulse represents a further abstraction from more biologically plausible conductance functions like the α function (Koch, 1999). However, the total conductance induced by a summation of independent conductance pulses tends to a gaussian distribution for a large number of input spikes, irrespective of the precise form of the conductance pulses. Therefore, the specific shape of the conductance function becomes of minor relevance for the case of a large number of inputs; only its effective amplitude and duration are relevant. For correlated inputs, the relevance of the specific conductance function depends on the size of the synchronization clusters with respect to the total number of inputs. Further abstraction of the conductance function to a delta peak leads to Stein's model with reversal potentials (Tuckwell, 1988), which was used in related studies of Feng and Brown (1999; Brown & Feng, 2000),

$$dU(t) = -\frac{(U(t) - E_r)}{\tau_m}\,dt + a_e(E_e - U(t))dn_e(t) + a_i(E_i - U(t))dn_i(t), \tag{6.1}$$

with $n_e(t)$ and $n_i(t)$ the number of excitatory and inhibitory input spikes, a_e and a_i weights of excitatory and inhibitory inputs and the meaning of the other variables as in section 2.1. Stein's model with reversal potentials is a first-order approximation of the conductance-based IF model, which holds well if the pulse duration of the synaptic conductance is much shorter than the effective membrane time constant. However, in the case of massive synaptic input, the effective time constant of the conductance-based IF model can be strongly reduced, such that the change in membrane potential

caused by an input spike is reduced in comparison with Stein's model with reversal potentials.

The conductance-based IF model has no spatial variation (it is a single-compartment model) or synaptic noise. Inclusion of such mechanisms would induce extra jitter in the output spiking (Tuckwell, 1988) and would reduce the cross-correlation between the firing of neurons with common input. Furthermore, it assumes a constant voltage threshold-passing mechanism for spike generation. In general, the dynamics of the stimulus determine whether this is a good model (Koch, Bernander, & Douglas, 1995). Reasonable agreement between the firing of a voltage-threshold leaky IF model and a compartmental model of a pyramidal cell was attained by Marsalek, Koch, & Maunsell (1997).

In conclusion, we consider the conductance-based IF model a suitable compromise between the numerical complexity of a compartmental neuron model with active gates (and the loads of parameters to be chosen) and the analytical tractability of the (oversimplified) nonleaky IF model.

6.2 Single Neuron Firing Characteristics. In this study, we did not make assumptions regarding the balance of excitatory and inhibitory effects in cortical neurons (as in the study by Shadlen & Newsome, 1998), but rather included a considerable variation of inhibitory versus excitatory contributions. Balance roughly depends on $(\lambda_i/\lambda_e) \times (N_i/N_e) \times (\hat{g}_i/\hat{g}_e) \times (\tau_i/\tau_e) \times (|E_i - E_t|/|E_e - E_t|)$ (see Troyer & Miller, 1997). This range of excitation versus inhibition was achieved by varying the excitatory and inhibitory firing rates $\lambda_{e,i}$, while the respective population sizes $N_{e,i}$, as well as the other parameters of the neuron model, were constant. For independent input spiking, the output firing depends on the effective firing rates $\lambda_{e,i}N_{e,i}$ and thus variations of $\lambda_{e,i}$ or $N_{e,i}$ are equivalent.

In line with related modeling studies (Shadlen & Newsome, 1998; Feng & Brown, 1999) we chose $N_e = N_i$, since this allowed us to use equal sizes of the synchronization clusters and the common input for excitatory and inhibitory synapses. However, it should be realized that anatomical studies show that the ratio of excitatory to inhibitory inputs of cortical neurons is typically about 9:1 (Braitenberg & Schüz, 1998). Notice that it would be easy to attain equal input and output firing rates in the model by choosing appropriate numbers of excitatory and inhibitory inputs. For example, since $\langle \text{ISI} \rangle = 10$ ms is attained for $\lambda_e = 100$ Hz, $N_e = 120$, $\lambda_i \approx 33$ Hz, and $N_i = 120$ (as is shown in Figure 4), choosing $\lambda_i = 100$ Hz and $N_i = 40$ results in equal input and output firing rates.

The derived expressions for the moments of the steady-state potential U_∞ and (to a lesser extent) the effective time constant τ_m provide a valuable link between the parameters of the conductance-based IF model and the input firing rates on the one hand and the output firing characteristics on the other hand. In particular, we found that the CV was about constant for a range of excitatory and inhibitory presynaptic firing rates if the excitation-

inhibition distribution was such that $\langle U_\infty \rangle = U_t + k\sigma(U_\infty)$ (see Figure 4). For $k = 0$, we observed CV ≈ 0.45, similar to results of Feng and Brown (1999) for the current-based IF model and Stein's model with reversal potentials. Furthermore, we found that for constant k, the induced firing rate increases as a function of the presynaptic firing rate, especially for small k.

The analysis of the effect of synchronization clusters was performed for an excitatory firing rate $\lambda_e = 100$ Hz and inhibitory firing rates $\lambda_i = 0$ and λ_i such that $\langle U_\infty \rangle = U_t + k\sigma(U_\infty)$ for $k \in \{-1, 0, 1\}$. The choice of the excitatory firing rate hardly affects CV, since CV was shown to be approximately constant for constant k. This choice affects the output firing rate, but we expect the observed trends to be valid for other excitatory firing rates as well.

A clear influence of the inhibitory firing rate was found on the dependence of the postsynaptic firing rate as a function of the input correlation. An increase in the firing rate of excitatory synchronous clusters for low to medium inhibitory input firing rates (leading to CV < 0.5) did not affect the output firing rate, but induced a clear increase in the output firing rate for high inhibitory input frequencies. Furthermore, the postsynaptic firing rate was found to be almost independent of the cluster size, especially for low to medium inhibitory firing rates. Input correlation thus affects the postsynaptic firing rate only if the inhibitory firing rate is sufficiently high.

In contrast to the effectuated firing rate, the variation of the interspike intervals increased with the input correlation for low to medium inhibitory firing rates and was often constant for large inhibitory firing rates. In addition to the cluster correlation K (Brown & Feng, 2000), the cluster size also appears to be an important determinant of the variation in the spiking times. To achieve CV > 1, both independent excitation and inhibition, as well as sufficiently large synchronous excitatory clusters, were essential, although the inhibitory firing rate could still be relatively low. In this case, the impact of the variations in the membrane potential due to the independent excitatory and inhibitory input, as well as due to the synchronization clusters, was sufficiently large to exceed the CV of a Poisson process.

The effects of the cluster correlation and the cluster size depend on the independent excitatory and inhibitory background spiking. Given constant effective frequencies $\lambda^b_{e,i} N_{e,i}$, the impact of a synchronization cluster on the membrane potential (and thus on postsynaptic firing) does not depend on the population sizes.

We considered correlation between excitatory inputs and/or between inhibitory inputs, but not between excitatory and inhibitory inputs. We expect that a positive correlation between excitatory and inhibitory inputs reduces the effective excitatory and inhibitory firing rates, since excitation and inhibition now tend to cancel each other. A negative correlation is expected to amplify the effect of excitatory input, since it implies that the probability that inhibitory input cancels the effect of excitatory input is reduced and thus the threshold potential can be reached earlier.

In this study, we assumed delta correlation between the firing times in a synchronization cluster, which was motivated by the notion that we did not want to introduce yet another (dispersion) parameter. Figures 6 through 8 show that the postsynaptic firing rate is not greatly affected by the sizes of the synchronization clusters (sizes from 12.5% to 100% of all inputs). In other words, it does not make a large difference whether all inputs receive a spike simultaneously or whether different synchronization clusters are used. Therefore, we do not expect that the "no dispersion" assumption affects our conclusions with respect to the postsynaptic firing rate to a large extent. Only for large inhibitory contributions may some effect of dispersion on the postsynaptic firing rate be expected. In contrast, dispersion of the firing times in a synchronization cluster is expected to have a significant impact on the CV. Therefore, the size of an excitatory synchronization cluster needed to induce a particular CV, as we found in this study, represents a lower bound of the required cluster size if dispersion of the input spikes is considered. Given the delta correlation, the results of this study already show that large synchronization clusters are likely to be necessary to achieve CV $>$ 1. Direct experimental evidence is needed to determine the size of synchronization clusters in vivo.

6.3 Cross-Correlation Due to Common and Synchronous Input. The cross-correlation between the firing of uncoupled neurons with common input depends on several parameters, such as the excitatory and inhibitory firing rates, the fraction of common input, and the presence of synchronization clusters in the input spike series. Interestingly, we found that common input may induce oscillatory cross-correlation patterns, which resemble the cross-correlation patterns obtained in measurements on neurons in the visual system encoding the same object (Singer & Gray, 1995). However, in our model, these oscillatory cross-correlation patterns were found only for small coefficients of variation (CV $<$ 0.5) in the output spiking, whereas CV $\approx$ 1 is usually measured for cortical neurons (Shadlen & Newsome, 1998).

We found that even in the artificial case of completely identical excitatory inputs, the maximum cross-correlation is strongly reduced by independent inhibitory firing to about $K_{xy}(0) = 0.09$. For 50% common excitatory input $K_{xy}(0) = 0.03$ and for assumingly even more realistic ratios of less than 20% common input, $K_{xy}(0)$ falls below 0.01. Interestingly, we found that the cross-correlation initially increases with increasing inhibitory firing rate but decreases again for large inhibitory firing rates. The incline of the cross-correlation is due to the increase in the importance of coincidental (common) excitatory firing to achieve postsynaptic firing for low and medium inhibitory firing rates. Its decline illustrates the rising importance of both a coincidental increase in (common) excitatory firing and a decrease in (independent) inhibitory firing for high inhibitory firing rates.

If, in addition to the excitatory input, the inhibitory input also is partly

common, the zero-time cross-correlation is increased to $K_{xy}(0) = 0.05$ for 50% common input and $K_{xy}(0) = 0.013$ for 20% common input. These values are likely to be optimistic, though, since noisy synaptic transmission will further diminish the cross-correlation.

Much higher cross-correlation can be achieved if (large) synchronization clusters exist in the input streams. For instance, if presynaptic spikes are part of a synchronization cluster 1 out of 10 times ($K = 0.1$), we found in our simulations $K_{xy}(0) \approx 0.06$ for 20% common input and $K_{xy}(0) \approx 0.20$ for 50% common input. Even if these correlations were attenuated by noisy synaptic transmissions, they still would represent significant coincidental firing, similar to experimentally obtained values of about $K_{xy}(0) \approx 0.08 - 0.10$ by Vaadia et al. (1995). Thus, if synchronization clusters are part of the common input, the output correlation can be sufficient to maintain synchronization clusters from one neural layer to the next. This conclusion is in line with the results of Diesmann et al. (1999), who furthermore reported on the required relation between the size of synchronization clusters and their dispersion such that synchrony can be maintained.

In conclusion, large fractions of common input would be required to induce significant correlations of output spikes of pairs of neurons for input streams without synchronization clusters, but only modest fractions would be required if synchronization clusters are part of the input spike streams if there exists no correlation between the excitatory and inhibitory inputs. Concerning the ontogenesis of synchronization clusters, this implies that they are unlikely to be generated by common input alone, but that lateral interactions are essential. Given the existence of sufficiently large synchronization clusters, significant postsynaptic synchronization may be maintained by common input.

Acknowledgments

We thank Martijn Leisink for his mathematical advice. We also acknowledge the useful comments of the reviewers, which led to an improvement of this article.

References

Braitenberg, V., & Schüz, A. (1998). *Cortex: Statistics and geometry of neuronal connectivity*. Berlin: Springer-Verlag.

Brown, D., & Feng, J. (2000). Impact of correlated inputs on the output of the integrate-and-fire models. *Neural Computation, 12*, 711–732.

Brunel, N., & Hakim, V. (1999). Fast global oscillations in networks of integrate-and-fire neurons with low firing rates. *Neural Computation, 11*, 1621–1671.

Bush, P., & Sejnowski, T. (1996). Inhibition synchronizes sparsely connected cortical neurons within and between columns in realistic network models. *Journal of Computational Neuroscience, 3*, 91–110.

Diesmann, M., Gewaltig, M-O., & Aertsen, A. (1999). Stable propagation of synchronous spiking in cortical neural networks. *Nature, 402*, 529–533.

Ermentrout, G. B., & Kopell, N. (1998). Fine structure of neural spiking and synchronization in the presence of conduction delays. *Proceedings of the National Academy of Sciences USA, 95*, 1259–1264.

Ernst, U., Pawelzik, K., & Geisel, T. (1998). Delay-induced multistable synchronization of biological oscillators. *Physical Review E, 57*, 2150–2162.

Feng, J., & Brown, D. (1999). Coefficient of variation of interspike intervals greater than 0.5. How and when? *Biological Cybernetics, 80*, 291–297.

Feng, J., Brown, D., & Li, G. (In press). Synchronization due to common pulsed input in Stein's model. *Physical Review E*.

Gerstner, W. (1998). Populations of spiking neurons. In W. Maas & C. M. Bishop (Eds.), *Pulsed neural networks* (pp. 261–295). Cambridge, MA: MIT Press.

Juergens, E., & Eckhorn, R. (1997). Parallel processing by a homogeneous group of coupled model neurons can enhance, reduce and generate signal correlations. *Biological Cybernetics, 76*, 217–227.

Kempter, R., Gerstner, W., van Hemmen, J. L., & Wagner, H. (1998). Extracting oscillations: Neuronal coincidence detection with noisy periodic spike input. *Neural Computation, 10*, 1987–2017.

Knight, B. W. (1972). Dynamics of encoding in a population of neurons. *Journal of General Physiology, 59*, 734–766.

Koch, C. (1999). *Biophysics of computation*. New York: Oxford University Press.

Koch, C., Bernarder, O., & Douglas, R. J. (1995). Do neurons have a voltage or a current threshold for action potential initiation? *Journal of Computational Neuroscience, 2*, 63–82.

Marsalek, P., Koch, C., & Maunsell, J. (1997). On the relationship between synaptic input and spike output jitter in individual neurons. *Proceedings of the National Academy of Sciences USA, 94*, 735–740.

Mason, A., Nicoll, A., & Stratford, K. (1991). Synaptic transmission between individual pyramidal neurons of the rat visual cortex in vitro. *Journal of Neuroscience, 11*(1), 72–84.

Matsumura, M., Chen, D., Sawaguchi, T., Kubota, K., & Fetz, E. E. (1996). Synaptic interactions between primate precentral cortex neurons revealed by spike-triggered averaging of intracellular membrane potentials in vivo. *Journal of Neuroscience, 16*(23), 7757–7767.

Philips, W. A., & Singer, W. (1997). In search of common foundations for cortical computation. *Behavioral and Brain Sciences, 20*, 657–722.

Protopapas, A. D., Vanier, M., & Bower, J. M. (1998). Simulating large networks of neurons. In C. Koch & I. Segev (Eds.), *Methods in neuronal modeling*. Cambridge, MA: MIT Press.

Riehle, A., Grün, S., Diesman, M., & Aertsen, A. (1997). Spike synchronization and rate modulation differentially involved in motor cortical function. *Science, 278*, 1950–1953.

Shadlen, M. N., & Newsome, W. T. (1998). The variable discharge of cortical neurons: Implications for connectivity, computation, and information coding. *Journal of Neuroscience, 18*(10), 3870–3896.

Singer, W., & Gray, C. M. (1995). Visual feature integration and the temporal correlation hypothesis. *Annual Review of Neuroscience, 18*, 555–586.

Troyer, T. W., & Miller, K. D. (1997). Physiological gain leads to high ISI variability in a simple model of a cortical regular spiking cell. *Neural Computation, 9*, 971–983.

Tuckwell, H. C. (1988). *Introduction to theoretical neurobiology: Vol. 2, nonlinear and stochastic theories*. Cambridge: Cambridge University Press.

Vaadia, E., Haalman, I., Abeles, M., Bergman, H., Prut, Y., Slovin, H., & Aertsen, A. (1995). Dynamics of neuronal interaction in the monkey cortex to behavioral events. *Nature, 373*(9), 515–518.

Vreeswijk, C. van (1996). Partial synchronization in populations of pulse-coupled oscillators. *Physical Review E, 54*, 5522–5537.

Received February 2, 2000; accepted October 10, 2000.